Uncooled 100-GBaud Directly Modulated Membrane Lasers on SiC Substrate

Suguru Yamaoka,
Nikolaos-Panteleimon (Pandelis) Diamantopoulos, *Senior Member, IEEE, Senior Member, OSA*, Hidetaka Nishi, Takuro Fujii, *Member, IEEE*, Koji Takeda, *Senior Member, IEEE*, Tatsurou Hiraki, *Member, IEEE*, Shigeru Kanazawa, *Senior Member, IEEE*, Takaaki Kakitsuka, *Member, IEEE*, and Shinji Matsuo, *Fellow, IEEE, Fellow, OSA*

(Top-Scored Paper)

***Abstract*—We investigate the temperature dependence of the dynamic characteristics of a 1.3-μm InGaAlAs-based directly modulated membrane laser on a SiC substrate. The laser is fabricated by combining direct wafer bonding of SiC and InP substrates using a very thin (~10 nm) oxide layer and epitaxial regrowth of a membrane InP layer on the InP/SiC template. The membrane laser structure on SiC with a high thermal conductivity (490 $Wm^{-1}K^{-1}$) and a moderate refractive index (~2.6) ensures both high thermal dissipation and a large optical confinement factor in the active region, which are ideal for increasing the relaxation oscillation frequency even at high operating temperatures. We further leverage the optical feedback effect from the output facet of a waveguide to enhance the bandwidth and enable signal modulation at 100 GBaud and beyond. Owing to the high relaxation oscillation frequency and the photon-photon resonance effect, it is possible to obtain a flat frequency response at temperatures ranging from 25 to 85 °C. The fabricated membrane laser on SiC with an active-region length of 50 μm exhibits 3 dB bandwidths of >110, 97, and 74 GHz at 25, 55, and 85 °C, respectively. We successfully demonstrate 2-km transmissions of 100-Gbit/s NRZ signals under uncooled conditions (25 to 85 °C). Furthermore, the laser is capable of 112-Gbit/s NRZ modulation at 85 °C.**

***Index Terms*—Direct modulation, optical communication, optical feedback, semiconductor lasers, SiC.**

I. Introduction

As THE amount of data is growing due to various Internet technologies, such as smartphones, cloud services, and the Internet of Things, it becomes increasingly important to develop optical transmitters in data centers that are as high-speed, energy-efficient, and compact as possible. In recent years, ultra-high-capacity Ethernet standards such as 800 Gigabit Ethernet and 1.6 Terabit Ethernet are being considered [1]. Accordingly, 100-GBaud-class modulation speed is crucial. Directly modulated lasers (DMLs) with uncooled operation are widely deployed in short-reach optical communication networks because they are cost-effective, energy-efficient, and compact. Hence, there is a strong need for uncooled 100-GBaud DMLs. However, the bandwidth of standard DMLs is limited to around 30 GHz at 25 °C, which has caused them to be used only as 50-GBaud-class optical transmitters [2], [3], [4], [5]. The DML bandwidth is intrinsically characterized by the relaxation oscillation frequency f_r, damping factor, and RC time constant, where the f_r is a major bottleneck. Note that the f_r is proportional to the square root of the differential gain, the optical confinement factor Γ, the internal quantum efficiency, and the current density above the threshold current density.

Two paths toward bandwidth enhancement of DMLs have been researched extensively. From the viewpoint of increasing the f_r and the intrinsic bandwidth of InGaAsP- and InGaAlAs-based lasers in the C- and O-bands, the first approach seeks to increase the differential gain by using strained multi-quantum wells (MQWs) [6]. Although this approach succeeded in improving the f_r, its value remained at around 20 GHz. The second approach is to use optical feedback techniques, including the detuned-loading and photon-photon resonance (PPR) effects, to generate optical filters and extra modes besides the lasing mode, which enhances the f_r itself and adds an extra peak in the frequency response [7], [8], [9], [10], [11], [12], [13], [14], [15], [16], [17]. By applying these effects, a 55-GHz bandwidth was achieved with distributed reflector (DR) lasers, whose intrinsic bandwidth was ~30 GHz, on an InP-based platform [13].

A unique approach to enhance the f_r is to increase the optical confinement factor Γ [18]. We previously proposed a membrane laser on a SiO_2/Si structure in which the optical light was

Manuscript received 15 November 2022; revised 13 January 2023; accepted 19 January 2023. Date of publication 24 January 2023; date of current version 9 June 2023. *(Corresponding author: Suguru Yamaoka.)*

Suguru Yamaoka, Nikolaos-Panteleimon (Pandelis) Diamantopoulos, Hidetaka Nishi, Takuro Fujii, Koji Takeda, Tatsurou Hiraki, Takaaki Kakitsuka, and Shinji Matsuo are with the NTT Device Technology Labs, NTT Corporation, Atsugi-shi, Kanagawa 243-0198, Japan (e-mail: suguru.yamaoka.hm@hco.ntt.co.jp; pandelis.diamantopoulos@ieee.org; hidetaka.nishi.sf@hco.ntt.co.jp; takuro.fujii.uc@hco.ntt.co.jp; koji.takeda.vk@hco.ntt.co.jp; tatsurou.hiraki.gu@hco.ntt.co.jp; t.kakitsuka@waseda.jp; shinji.matsuo.vm@hco.ntt.co.jp).

Shigeru Kanazawa is with the NTT Device Technology Labs, NTT Corporation, Atsugi-shi, Kanagawa 243-0198, Japan, and also with the NTT Device Innovation Center, NTT Corporation, Atsugi-shi, Kanagawa 243-0198, Japan (e-mail: shigeru.kanazawa.vn@hco.ntt.co.jp).

Color versions of one or more figures in this article are available at https://doi.org/10.1109/JLT.2023.3239614.

Digital Object Identifier 10.1109/JLT.2023.3239614

This work is licensed under a Creative Commons Attribution-NonCommercial-NoDerivatives 4.0 License. For more information, see https://creativecommons.org/licenses/by-nc-nd/4.0/

strongly confined in the active membrane core, which was sandwiched by low-refractive-index materials such as air and SiO_2 [19], [20]. In addition, because the membrane laser included a surface grating with a high coupling coefficient, we could use a short cavity. Owing to Γ being three times higher than standard DMLs and the active region being 50 μm long, we obtained a high modulation efficiency of 9.4 GHz/mA$^{1/2}$ and a low energy cost of 132 fJ/bit with 25.8-Gbit/s non-return-to-zero (NRZ) signal modulation [20]. Although this laser had significant advantages in terms of energy efficiency, its f_r and f_{3dB} were as large as those of standard DMLs, at ~20 and ~30 GHz, respectively. The 2-μm-thick SiO_2 layer beneath the active region caused the temperature to rise considerably when the bias current (I_b) was increased. This resulted in an insufficient bias current to obtain higher f_r values.

To solve this, we proposed membrane lasers on a SiC substrate [14], which has a high thermal conductivity of 490 $Wm^{-1}K^{-1}$ [21] and a refractive index of ~2.6 in the O-band [22]. In the active region, high thermal dissipation and a high optical confinement factor can be achieved simultaneously, and the f_r and f_{3dB} are increased to 42 and 60 GHz at 25 °C, respectively. Furthermore, by using the PPR effect with a frequency of ~ 95 GHz, the f_{3dB} was enlarged to 108 GHz, thus enabling the laser to operate at 256 Gbit/s with four-level pulse-amplitude modulations (PAM-4) [14]. In addition, we achieved the net >300-Gbit/s/λ modulations using advanced digital signal processing technique [23]. However, these results were obtained at 25 °C, and there has been no demonstration of 100-GBaud modulations of any DML at a temperature higher than 25 °C. The next challenge is thus to achieve high-temperature 100-GBaud operation; however, it is challenging to achieve a flat small-signal response with the PPR effect because the f_r decreases at high temperatures [16], [17], mainly because of degradation of the differential gain. There is also an issue of how the PPR frequency changes with temperature [17]. In principle, membrane lasers on high-thermal-conductivity SiC are ideal for achieving a high f_r and f_{3dB} even at high temperatures because of the small self-heating effect, which reduces the degradation of the differential gain.

In our recent preliminary work [24], we demonstrated the record dynamic modulation characteristics of a membrane DR laser on SiC, including small-signal (S_{21}) responses at 25, 55, and 85 °C, with f_{3dB} values of >110, 97, and 74 GHz, respectively; moreover, we demonstrated 2-km transmissions of 100-Gbit/s NRZ signals at 25 and 85 °C for the first time. In this paper, we extend our previous results by incorporating static lasing properties that explain the mode transition with respect to the bias current and environmental temperature, which are of great importance for understanding the mechanism of the PPR effect. We further evaluate the bit-error-rate (BER) for (i) 100-Gbit/s NRZ signals at 55 °C to examine the uncooled condition ranging from 25 to 85 °C and (ii) 112-Gbit/s NRZ signals at 85 °C to examine the achievable modulation speed.

The rest of the paper is organized as follows. Following this introduction, the design and the fabrication process of the membrane laser on SiC are described in Section II. Section III presents the experimental results, including the fundamental static characteristics and dynamic modulation characteristics. Finally, Section IV concludes the paper.

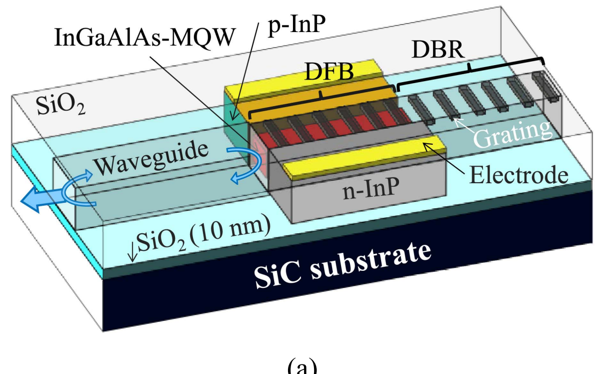

(a)

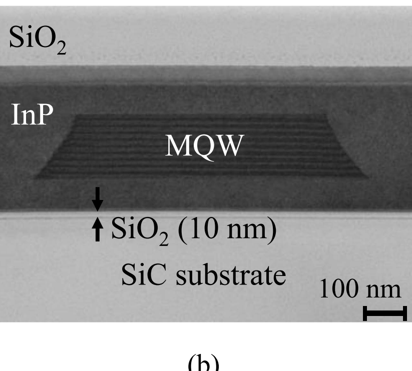

(b)

Fig. 1. (a) Schematic bird's-eye view of the membrane DR laser on a SiC substrate. (b) Cross-sectional TEM image of the DFB section.

II. Design and Fabrication

We designed a DR laser structure consisting of a distributed feedback (DFB) section, a distributed Bragg reflector (DBR) mirror, and a passive InP waveguide, where the lengths were 50, 60, and 135 μm, respectively (Fig. 1(a)). A cross-sectional transmission electron microscope (TEM) image of the DFB section is shown in Fig. 1(b). The total thickness of the III-V layer was ~340 nm. The active region comprised a 9-period InGaAlAs MQW and had a width of ~0.7 μm. We used a 10-nm-thick SiO_2 bonding layer, whereas the thickness was 40 nm in our previous work [14]. A thinner SiO_2 layer is better to reduce thermal dissipation and thus achieve high-temperature operation. We fabricated a lateral *p-i-n* structure that enabled lateral current injection, which has the advantage of reducing the RC time constant by reducing the pad-electrode capacitances. We formed uniform gratings on the InP surface, because they can avoid spatial localization of the optical power distribution (i.e., the spatial hole burning effect), in contrast to λ/4-shifted gratings [25]. The grating coupling coefficient was designed to be 600 cm^{-1}, giving a photon lifetime of ~1 ps. This short photon lifetime reduces the damping effect and maximizes the achievable f_{3dB} [14]. In this work, we designed the detuning

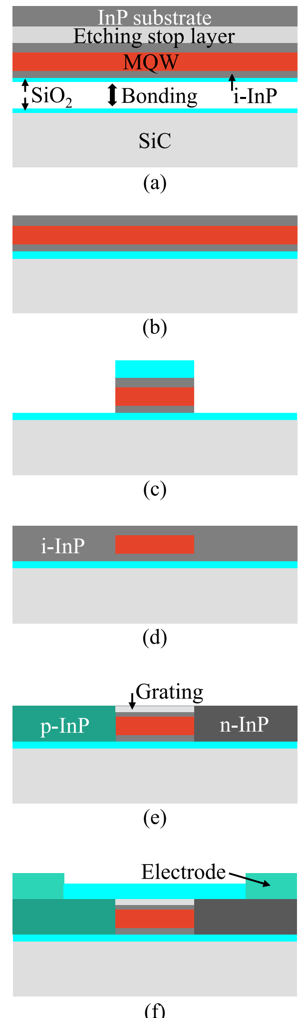

Fig. 2. Fabrication procedure of the membrane laser on a SiC substrate.

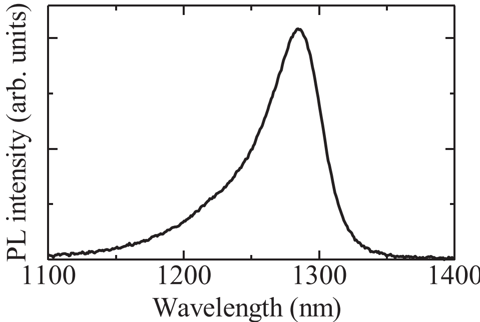

Fig. 3. PL spectrum of the InGaAlAs MQW buried in the InP membrane layer, obtained at 25 °C.

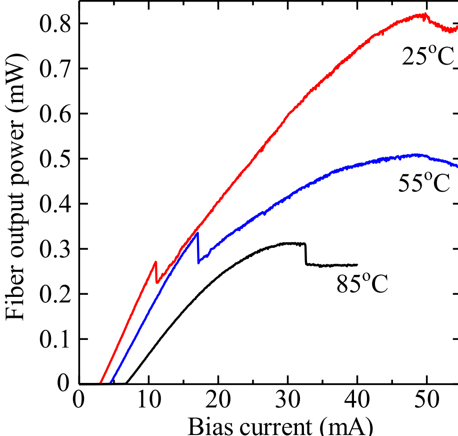

Fig. 4. L-I curves at 25, 55, and 85 °C.

between the photoluminescence (PL) peak wavelength and the lasing wavelength to be ∼10 nm at 25 °C.

As shown in Fig. 1(a), the reflection occurring between the waveguide's output facet and the front of the DFB section induces Fabry-Pérot (FP) interference. The PPR effect is caused by the interaction of the lasing mode and one of the FP modes, and the frequency response is enhanced at the frequency difference between the two modes. The free spectral range (FSR) of the FP modes was set to 270 GHz by using a 135-μm-long output waveguide.

The fabrication procedure is shown in Fig. 2. A 310-nm-thick membrane layer, which included 9-period InGaAlAs MQWs and an InGaAs etching stop layer, was grown on a 2-inch InP (001) substrate by metal–organic vapor phase epitaxy (MOVPE). We sputtered a 5-nm-thick SiO_2 bonding layer on both InP and SiC surfaces to yield a total thickness of 10 nm (Fig. 2(a)). After that, the InP and SiC substrates were bonded by oxygen-plasma-assisted direct bonding (Fig. 2(a)). Then, by using an etching stop layer, we selectively removed the InP substrate by mechanical and wet etching (Fig. 2(b)). Next, to define the core, a mesa-stripe structure was formed by dry/wet etching with a SiO_2 mask (Fig. 2(c)). Then, the core was buried in an intrinsic InP layer through epitaxial regrowth by MOVPE (Fig. 2(d)). Si-ion implantation and Zn thermal diffusion were applied to form the lateral *p-i-n* junction, after which surface gratings were formed on the top InP region for the DFB and DBR sections (Fig. 2(e)). Finally, contact metals were deposited on the n-InP and p-InP (Fig. 2(f)).

Fig. 3 shows the PL spectrum of the InGaAlAs-MQW buried in the InP membrane layer. It was obtained at 25 °C after the regrowth process, with an excitation wavelength of 1064 nm. We succeeded in observing PL from the active region on SiC. The PL peak wavelength was ∼1284 nm; thus, the DFB lasing wavelength at 25 °C was set to ∼1294 nm.

III. Results and Discussion

The output light versus bias current (L-I curve) at 25, 55, and 85 °C is shown in Fig. 4. The stage temperature was controlled by a thermoelectric cooler. A lensed fiber was used to collect the optical output power. The threshold currents at 25, 55, and 85 °C were evaluated as 2.9, 4.4, and 6.7 mA, respectively. A kink was observed around the PPR region at each temperature, with bias currents of 11.0, 17.1, and 32.5 mA at 25, 55, and 85 °C, respectively. The PPR-based bandwidth enhancement effect was observed in the current range slightly before the kink. The maximum optical output power coupled to the fiber was

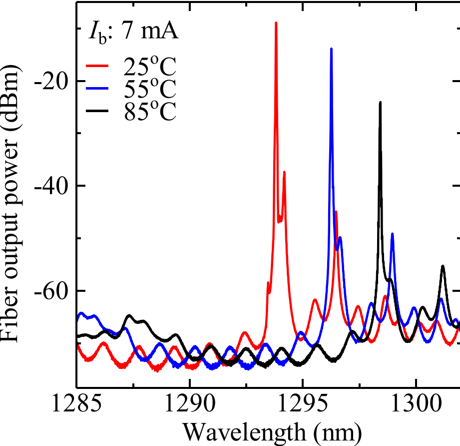

Fig. 5. Lasing spectra at 25, 55, and 85 °C, obtained with a bias current of 7 mA.

0.82, 0.51, and 0.31 mW at 25, 55, and 85 °C, respectively. The output power directly detected by a photodetector was ∼3 mW at 25 °C, which gives a fiber coupling loss of 5.6 dB. Note that the loss can be reduced by integrating a spot-size converter (SSC), which was used for the membrane laser on Si [26].

The lasing spectra at 25, 55, and 85 °C, obtained at a bias current of 7 mA, are shown in Fig. 5. Single-mode lasing was achieved for all temperatures by the rear DBR selecting the longer side mode of the DFB stopband. The optical feedback from the output facet generates FP modes, and the closest of these to the lasing mode on the long-wavelength side can act as the PPR mode. The reflectance at the facet was estimated to be ∼5% from fitting of the ripples in the stopband. Image maps of the lasing spectra as a function of the bias current at 25, 55, and 85 °C are shown in Fig. 6(a)–(c), respectively. As the DFB section's temperature was increased by increasing the bias current, the lasing mode was largely red-shifted. In contrast, the red shift of the FP modes was insignificant, because those modes are mainly defined by the passive feedback section. Thus, by increasing the bias current, the frequency separation between the lasing mode and the first long-wavelength FP mode becomes smaller. As a result, the magnitude of the frequency response becomes significant at a given frequency separation, and mode hopping was observed when the current was further increased, as shown in Fig. 6(a)–(c). The currents for mode hopping almost corresponded to those for the kinks observed in the L-I curves (Fig. 4). The temperature dependence of the initial frequency separation of the lasing mode and the nearest long-wavelength FP mode is depicted in Fig. 6(d). Note that the separation derived from the spectrum around the threshold current, where the temperature increase due to the self-heating effect is small. As shown in the figure, the initial frequency separation increased with the temperature. A possible reason for the larger detuning at higher temperatures is that the threshold carrier density increases with temperature, resulting in a larger blue shift, due to carrier effects, of the lasing mode. In addition, the temperature dependencies of the effective refractive indices of the InP waveguide and the MQW core, which are respectively

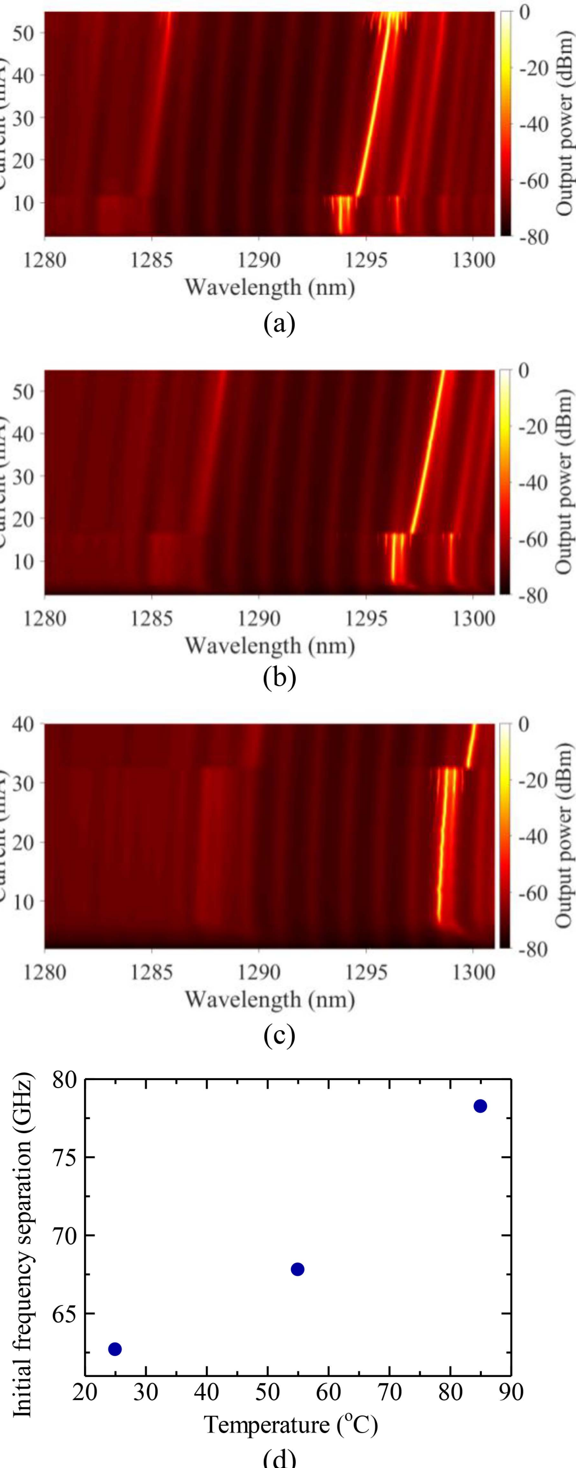

Fig. 6. Image maps of the lasing spectra as a function of the bias current at (a) 25, (b) 55, and (c) 85 °C. (d) Temperature dependence of the initial frequency separation between the lasing mode and the nearest long-wavelength FP mode.

responsible for the FP and DFB modes, are slightly different. The increased currents at the kinks in Fig. 4 originate from the fact that the initial frequency separation increased with temperature, and a larger current was thus required to reach the mode-hopping condition.

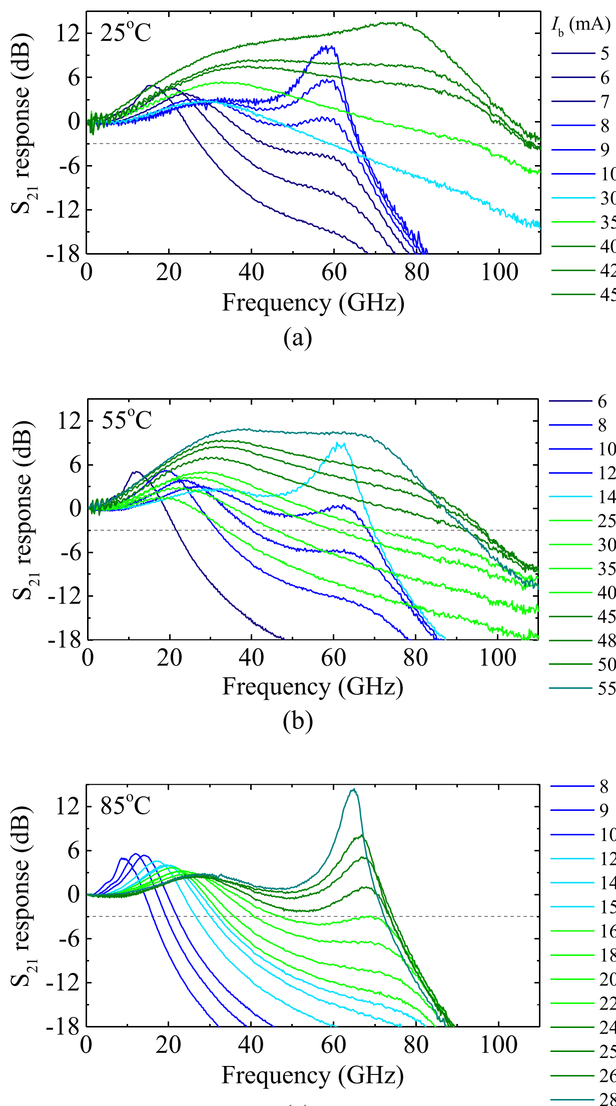

Fig. 7. Small-signal S_{21} responses at (a) 25, (b) 55, and (c) 85 °C.

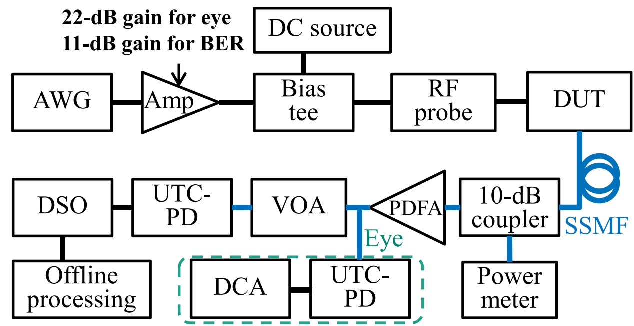

Fig. 8. Experimental setup for evaluating the eye diagrams and BERs. DUT: Device under test.

Hereafter, we show the dynamic modulation characteristics. The small-signal S_{21} responses at 25, 55, and 85 °C are shown in Fig. 7(a)–(c), respectively. A light component analyzer (Keysight N4372E) capable of operation up to 110 GHz was used for these measurements. At 25 and 55 °C, two PPR-occurrence regions were observed in two bias current regions below the currents at the kinks. At 85 °C, only the first PPR-occurrence region was observed, because the current range of the second region was above the current at the thermal rollover, and the output power (i.e., the feedback power) was insufficient. In the temperature range from 25 to 85 °C, relatively flat frequency responses were obtained, with the following $f_{3\mathrm{dB}}$ values: 66 GHz at 9 mA and >110 GHz at 45 mA for 25 °C; 70 GHz at 14 mA and 97 GHz at 50 mA for 55 °C; and 74 GHz at 26 mA for 85 °C. To the best of our knowledge, these $f_{3\mathrm{dB}}$ values are all records for DMLs. Note that membrane lasers on SiO_2/Si using the PPR effect exhibited $f_{3\mathrm{dB}}$ values of 60, 54, and 46 GHz at 25, 50, and 70 °C respectively [17]. In comparison, this membrane laser on SiC with an f_{r} peak of around 30 GHz and $f_{3\mathrm{dB}}$ of 74 GHz at 85 °C demonstrates that the high thermal conductivity of SiC helped suppress degradation of the differential gain with increasing bias current.

Here, we discuss the temperature dependence of the PPR frequency. For the fabricated device in this work, the PPR frequency in the first PPR-occurrence region increased with temperature, as shown in Fig. 7(a)–(c). Depending on the bias current above threshold, the degradation of the gain at higher temperatures [19] causes a variation in the photon density. Therefore, the blue-shift due to the adiabatic chirp changes with the temperature and the bias current [6]. As shown in Fig. 4, the output power at the kink was independent of temperature and the output power for the first PPR-occurrence region increased with temperature. In addition to this, the initial frequency separation increases with temperature (Fig. 6(d)). Therefore, under these conditions, the PPR frequency can increase with temperature. This effectively means that, when the output power before the kink increases (decreases), the PPR side-mode receives sufficient feedback power to enhance the modulation response at more distant (closer) frequency from the main lasing mode. In fact, for the membrane lasers on the membrane laser on SiO_2/Si, the output power at the kink decreased with temperature, resulting in the reduced PPR frequency [17]. In the small-signal responses using the first PPR regions (i.e., <30 mA) as shown in Fig. 7(a)–(c), we achieved almost the same f_{r} values over the temperature range from 25 to 85 °C. These results indicate that SiC successfully suppresses the temperature increase caused by current injection.

The experimental setup for evaluating optical eye diagrams and BERs is shown in Fig. 8. First, 100-Gbit/s and 112-Gbit/s NRZ signals with a pseudorandom binary sequence of 2^{15}-1 were generated by an arbitrary waveform generator (AWG) at 200 GSa/s with an analog $f_{3\mathrm{dB}}$ of 70 GHz (Keysight M8199A). A 66-GHz electrical amplifier with a 22-dB gain (SHF M804B) and a 65-GHz electrical amplifier with an 11-dB gain (SHF 827) were used for measuring the respective eye diagrams and BERs. The RF and DC signals were combined using a 65-GHz bias tee, and the DML was driven by a 67-GHz RF probe. The optical power coupled to a standard single-mode fiber (SSMF) was monitored with a 10-dB coupler. The signals were amplified by a praseodymium-doped fiber amplifier (PDFA), and an in-house unitraveling-carrier photodiode (UTC-PD) module with

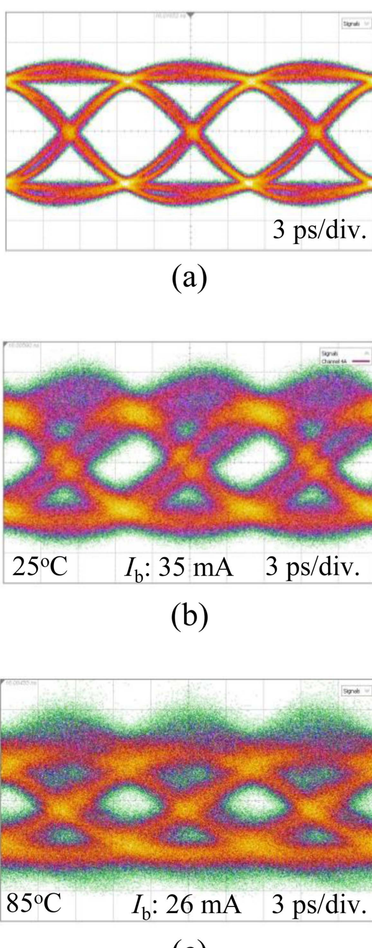

Fig. 9. (a) Input 100-Gbit/s NRZ electrical eye diagram. Optical eye diagrams obtained for 100-Gbit/s NRZ signals at (b) 25 and (c) 85 °C. A pre-emphasis filter was used at the AWG on the transmitter side, whereas no equalizer was used on the receiver side.

an $f_{3\mathrm{dB}}$ of >67 GHz was used for detection. The eye diagrams were acquired with a digital communication analyzer (DCA). For the BER measurements, the received electrical signal with the UTC-PD followed by controlling the power by a variable optical attenuator (VOA) was captured by a real-time digital storage oscilloscope (DSO). The DSO had a sampling rate of 160 GSa/s and an $f_{3\mathrm{dB}}$ of ∼63 GHz. For the eye measurements with the DCA, a pre-emphasis filter at the AWG was used to mitigate the RF impairment of the electrical components. This allowed us to obtain inherent optical eye diagrams reflecting only the laser frequency response (no equalizer was used on the receiver side). We obtained the input 100-Gbit/s NRZ electrical eye diagram with a clear eye opening, as shown in Fig. 9(a). For the BER measurements, an 11-tap linear equalizer and a 6-tap decision-feedback equalizer were used to compensate for distortions in the eye diagrams on the receiver side, whereas the pre-emphasis filter was not used at the AWG on the transmitter side.

The 100-Gbit/s NRZ optical eye diagrams obtained at 25 and 85 °C are shown in Fig. 9(b) and (c), respectively. The respective bias current, bias voltage, and peak-to-peak voltage V_{pp} were 35 mA, 2.97 V, and 1.64 V at 25 °C, and 26 mA, 2.43 V, and 1.17 V at 85 °C. We obtained clear eye openings at 25 and 85 °C with extinction ratios of 3.3 and 2.9 dB, respectively. This result demonstrates the DML's large bandwidth.

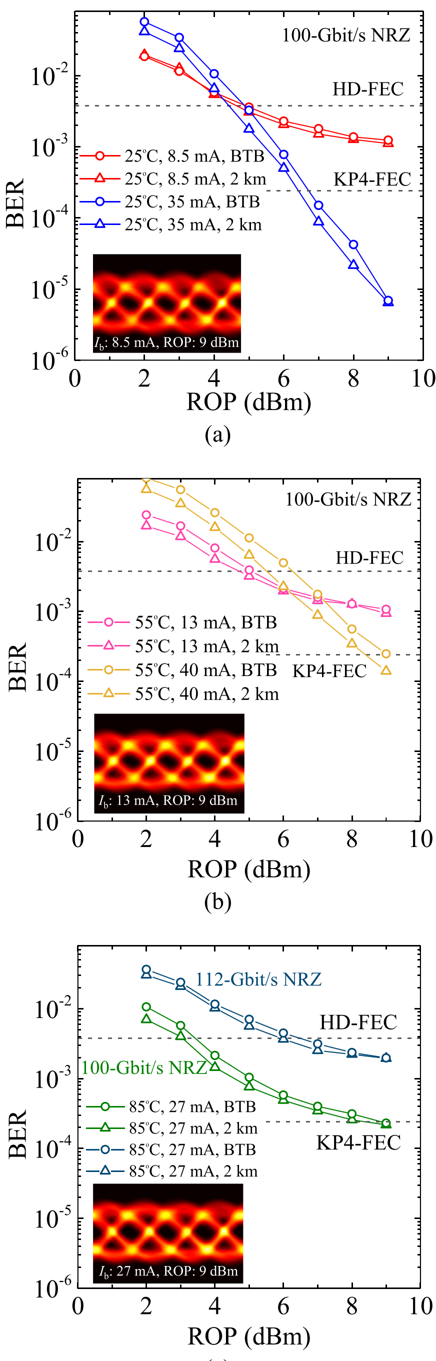

Fig. 10. BER as a function of the ROP at (a) 25, (b) 55, and (c) 85 °C. Insets: Equalized optical eye diagrams for 100-Gbit/s NRZ signals. An 11-tap linear equalizer and a 6-tap decision-feedback equalizer were used on the receiver side, whereas no pre-emphasis filter was used at the AWG on the transmitter side.

Next, the BERs at 25, 55, and 85 °C are shown in Fig. 10(a)–(c), respectively, as a function of the received optical power (ROP) for back-to-back (BTB) and 2-km transmissions of 100-Gbit/s NRZ signals. The insets show equalized optical eye

diagrams for 100-Gbit/s NRZ signals, for which we modulated the laser at the first PPR-occurrence region. We evaluated the BER from both the first and second PPR-occurrence regions at 25 and 55 °C, but only from the first region at 85 °C. At 25 °C, the BERs obtained at a current of 8.5 mA and a V_{pp} of 0.4 V were less than the 7%-overhead hard-decision forward error correction (HD-FEC) threshold of 3.8×10^{-3} [27]. Meanwhile, the BERs obtained at 35 mA and a V_{pp} of 1.1 V were less than the 5.8%-overhead KP4-FEC threshold of 2.4×10^{-4} [28]. At 55 °C, the BERs obtained at 13 (40) mA and a V_{pp} of 0.6 (1.1) V were less than the HD-FEC (KP4) threshold. At 85 °C, the BERs obtained at 27 mA and a V_{pp} of 1.1 V were less than the KP4-FEC threshold. The temperature of the active region was calculated from the change in the lasing wavelength with respect to the injected electrical power, and it was estimated to be 97 °C at a bias current of 27 mA. Furthermore, at 85 °C, we increased the bit rate to 112-Gbit/s NRZ and evaluated the BERs, which were still less than the HD-FEC threshold. Thus, these results demonstrate uncooled 100-Gbits/s NRZ operation at temperatures from 25 to 85 °C. Note that the lower BERs after 2-km transmission as compared to BTB transmission were presumably due to the SSMF's negative dispersion [29]. For the first PPR-occurrence region, the energy costs at 25, 55 and 85 °C were calculated as 139, 249, and 708 fJ/bit, respectively, thus demonstrating operation with low power consumption. Note that the fiber-coupled output power was still insufficient, and the PDFA was thus required. To address this issue, in the future we plan to integrate an SSC, increase the active length, and optimize the fabrication processes that might degrade the gain.

IV. Conclusion

We have investigated the high-temperature operation characteristics of a membrane DR laser on a SiC substrate with high thermal conductivity and a moderate refractive index. Because of the high thermal dissipation and the optical confinement factor, a high f_r was maintained at temperatures up to 85 °C. By incorporating the PPR effect, we succeeded in obtaining a maximum f_{3dB} of >110 GHz at 25 °C, 97 GHz at 55 °C, and 74 GHz at 85 °C. The device demonstrated 2-km transmission of a 100-Gbit/s NRZ signal at 25, 55, and 85 °C. These results represent record performance and thus demonstrate the potential of DMLs on SiC for uncooled 100-GBaud operation at 800 Gbit/s, 1.6 Tbit/s, and beyond.

References

[1] "200G per lane for future 800G & 1.6T modules," 800G Pluggable Multi-Source Agreement (MSA), 2021. [Online]. Available: https://www.800gmsa.com/documents/200g-per-lane-for-future-800g-and-16t-modules

[2] T. Simoyama, M. Matsuda, S. Okumura, A. Uetake, M. Ekawa, and T. Yamamoto, "50-Gbps direct modulation using 1.3-µm AlGaInAs MQW distribute-reflector lasers," in *Proc. IEEE 38th Eur. Conf. Exhib. Opt. Commun.*, 2012, pp. 1–3.

[3] W. Kobayashi et al., "50-Gb/s direct modulation of a 1.3-µm InGaAlAs-based DFB laser with a ridge waveguide structure," *IEEE J. Sel. Topics Quantum Electron.*, vol. 19, no. 4, Jul./Aug. 2013, Art. no. 1500908,.

[4] K. Nakahara et al., "Direct modulation at 56 and 50 Gb/s of 1.3-µm InGaAlAs ridge-shaped-BH DFB lasers," *IEEE Photon. Technol. Lett.*, vol. 27, no. 5, pp. 534–536, Mar. 2015.

[5] N. Sasada et al., "Wide-temperature-range (25–80 °C) 53-Gbaud PAM4 (106-Gb/s) operation of 1.3-µm directly modulated DFB lasers for 10-km transmission," *J. Lightw. Technol.*, vol. 37, no. 7, pp. 1686–1689, Apr. 2019.

[6] Y. Matsui, "Directly modulated laser technology: Past, present, and future," in *Datacenter Connectivity Technologies: Principles and Practice*. Gistrup, Denmark: River Publishers, 2018, ch. 3, pp. 87–172.

[7] O. Kjebon, R. Schatz, S. Lourdudoss, S. Nilsson, B. Stalnacke, and L. Backbom, "30 GHz direct modulation bandwidth in detuned loaded InGaAsP DBR lasers at 1.55 µm wavelength," *Electron. Lett.*, vol. 33, no. 6, pp. 488–489, Mar. 1997.

[8] L. Bach, W. Kaiser, J. P. Reithmaier, A. Forchel, T. W. Berg, and B. Tromborg, "Enhanced direct-modulated bandwidth of 37 GHz by a multisection laser with a coupled-cavity-injection-grating design," *Electron. Lett.*, vol. 39, no. 22, pp. 1592–1593, Oct. 2003.

[9] U. Troppenz et al., "40 Gb/s directly modulated InGaAsP passive feedback DFB laser," in *Proc. 32nd Eur. Conf. Opt. Commun.*, 2006, Paper T4.5.5.

[10] J. Kreissl, V. Vercesi, U. Troppenz, T. Gaertner, W. Wenisch, and M. Schell, "Up to 40 Gb/s directly modulated laser operating at low driving current: Buried-heterostructure passive feedback laser (BH-PFL)," *IEEE Photon. Technol. Lett.*, vol. 24, no. 5, pp. 362–364, Mar. 2012.

[11] H. Dalir and F. Koyama, "High-speed operation of bow-tie-shaped oxide aperture VCSELs with photon–photon resonance," *Appl. Phys. Exp.*, vol. 7, no. 2, Jan. 2014, Art. no. 022102.

[12] A. Abbasi et al., "Direct and electroabsorption modulation of a III–V-on-silicon DFB laser at 56 Gb/s," *IEEE J. Sel. Topics Quantum Electron.*, vol. 23, no. 6, Nov./Dec. 2017, Art. no. 1501307.

[13] Y. Matsui et al., "55 GHz bandwidth distributed reflector laser," *J. Lightw. Technol.*, vol. 35, no. 3, pp. 397–403, Feb. 2017.

[14] S. Yamaoka et al., "Directly modulated membrane lasers with 108 GHz bandwidth on a high-thermal-conductivity silicon carbide substrate," *Nature Photon.*, vol. 15, no. 1, pp. 28–35, Jan. 2021.

[15] Y. Matsui, R. Schatz, D. Che, F. Khan, M. Kwakernaak, and T. Sudo, "Low-chirp isolator-free 65-GHz-bandwidth directly modulated lasers," *Nature Photon.*, vol. 15, no. 1, pp. 59–63, Jan. 2021.

[16] N.-P. Diamantopoulos et al., "47.5 GHz membrane-III-V-on-Si directly modulated laser for sub-pJ/bit 100-Gbps transmission," *Photonics*, vol. 8, no. 2, Jan. 2021, Art. no. 31.

[17] N.-P. Diamantopoulos et al., "60 GHz bandwidth directly modulated membrane III-V lasers on SiO_2/Si," *J. Lightw. Technol.*, vol. 40, no. 10, pp. 3299–3306, May 2022.

[18] T. Okamoto, N. Nunoya, Y. Onoda, T. Yamazaki, S. Tamura, and S. Arai, "Optically pumped membrane BH-DFB lasers for low-threshold and single-mode operation," *IEEE J. Sel. Topics Quantum Electron.*, vol. 9, no. 5, pp. 1361–1366, Sep./Oct. 2003.

[19] S. Matsuo and T. Kakitsuka, "Low-operating-energy directly modulated lasers for short-distance optical interconnects," *Adv. Opt. Photon.*, vol. 10, no. 3, pp. 567–643, Sep. 2018.

[20] H. Nishi et al., "Membrane distributed-reflector laser integrated with SiO_x-based spot-size converter on Si substrate," *Opt. Exp.*, vol. 24, no. 16, pp. 18346–18352, Aug. 2016.

[21] T. Kimoto and J. A. Cooper, *Fundamentals of Silicon Carbide Technology: Growth, Characterization, Devices and Applications*. Hoboken, NJ, USA: Wiley, 2014.

[22] C. Xu et al., "Temperature dependence of refractive indices for 4H- and 6H-SiC," *J. Appl. Phys.*, vol. 115, Mar. 2014, Art no. 113501.

[23] N.-P. Diamantopoulos et al., ">100-GHz bandwidth directly-modulated lasers and adaptive entropy loading for energy-efficient >300-Gbps/λ IM/DD systems," *J. Lightw. Technol.*, vol. 39, no. 3, pp. 771–778, Feb. 2021.

[24] S. Yamaoka et al., "Uncooled 100-GBaud operation of directly modulated membrane lasers on high-thermal-conductivity SiC substrate," in *Proc. IEEE 48th Eur. Conf. Opt. Commun.*, 2022, pp. 1–4.

[25] K. Nakahara, Y. Wakayama, T. Kitatani, T. Fukamachi, Y. Sakuma, and S. Tanaka, "1.3 µm InGaAlAs asymmetric corrugation-pitch-modulated DFB lasers with high mask margin at 28 Gbit/s," *Electron. Lett.*, vol. 50, no. 13, pp. 947–948, Jun. 2014.

[26] T. Fujii et al., "1.3-µm directly modulated membrane laser array employing epitaxial growth of InGaAlAs MQW on InP/SiO_2/Si substrate," in *Proc. IEEE 42nd Eur. Conf. Exhib. Opt. Commun.*, 2016, pp. 1–3.

[27] L. M. Zhang and F. R. Kschischang, "Staircase codes with 6% to 33% overhead," *J. Lightw. Technol.*, vol. 32, no. 10, pp. 1999–2002, May 2014.

[28] *IEEE Standard for Ethernet - Amendment 10: Media Access Control Parameters, Physical Layers, and Management, Parameters for 200 Gb/s and 400 Gb/s Operation*, IEEE Standard 802.3bs-2017, Dec. 2017.

[29] N.-P. Diamantopoulos, W. Kobayashi, H. Nishi, K. Takeda, T. Kakitsuka, and S. Matsuo, "Amplifierless PAM-4/PAM-8 transmissions in O-band using a directly modulated laser for optical data-center interconnects," *Opt. Lett.*, vol. 44, no. 1, pp. 9–12, Dec. 2019.

Suguru Yamaoka was born in Osaka, Japan, in 1993. He received the B.E., M.E., and Ph.D. degrees in applied physics from Osaka City University, Osaka, Japan, in 2015, 2017, and 2021, respectively. In 2017, he joined NTT Device Technology Labs, Atsugi, Japan. His research interests include high-speed and low-power-consumption directly modulated semiconductor lasers. He is a Member of the IEICE and Japanese Society of Applied Physics.

Nikolaos-Panteleimon (Pandelis) Diamantopoulos (Senior Member, IEEE) was born in Athens, Greece, in 1988. He received the B.Sc. degree from the University of Peloponnese, Tripoli, Greece, in 2009, the two M.Sc. degrees from Aston University, U.K., and Scuola Superiore Sant'Anna Pisa, Pisa, Italy, in 2012, under the joint-masters Erasmus Mundus Program, and the Ph.D. degree from Osaka University, Osaka, Japan, in 2016. Between 2011 and 2016, he was involved in several EU-funded R&D Projects, Athens Information Technology (AIT) Research Center, Greece. Since 2016, he has been with NTT Device Technology Labs, Japan. His research interests include integrated photonics, optical communications, digital signal processing, neuromorphic systems, space-division multiplexing, and semiconductor lasers. He is a Senior Member of Optica (formerly OSA).

Hidetaka Nishi received the B.S. and M.S. degrees in mechanical science and engineering and the Ph.D. degree in electronics and applied physics from the Tokyo Institute of Technology, Tokyo, Japan, in 2005, 2007, and 2016, respectively. In 2007, he joined NTT Microsystem Integration Laboratories. Since then, he has been conducting research on integrated photonic and plasmonic devices. He is a Member of The Optical Society and Japanese Society of Applied Physics.

Takuro Fujii (Member, IEEE) was born in Kyoto, Japan, in 1986. He received the B.E. and M.E. degrees in system design engineering from Keio University, Kanagawa, Japan, in 2010 and 2012, respectively. In 2012, he joined NTT Photonics Laboratories, Atsugi, Japan. He has been researching MOVPE growth of III–V semiconductors and the development of III–V semiconductor lasers on Si for photonic integrated circuits. He is a Member of the Institute of Electronics, Information and Communication Engineers and the Japanese Society of Applied Physics (JSAP). He was the recipient of the Young Scientist Presentation Award from the JSAP in 2014.

Koji Takeda (Senior Member, IEEE) received the B.S., M.S., and Ph.D. degrees in electronics engineering from the University of Tokyo, Tokyo, Japan, in 2005, 2007, and 2010, respectively. In 2010, he joined NTT Photonics Laboratories. His research interests include ultralow-power optical interconnects, InP photonic integrated circuits, and photonic crystal lasers. He is a Member of the IEICE and JSAP. From 2008 to 2010, he received a research fellowship for young scientists from the Japan Society for the Promotion of Science (JSAP). He was the recipient of the Best Student Paper Award from the IEEE Photonics Society in 2009 and the Outstanding Student Presentation Award from the JSAP in 2010.

Tatsurou Hiraki (Member, IEEE) received the B.E., M.E., and Ph.D. degrees from Tohoku University, Sendai, Japan, in 2009, 2011, and 2017, respectively. In 2011, he joined NTT Microsystem Integration Laboratories, Nippon Telegraph and Telephone Corporation, Japan. His research interests include heterogeneously integrated III-V semiconductor optical modulators, optical amplifiers, and laser diodes on Si photonics circuits. He is a Member of the Institute of Electronics, Information, and Communication Engineers, and Japan Society of Applied Physics.

Shigeru Kanazawa (Senior Member, IEEE) received the B.E., M.E., and Ph.D. degrees in electronic engineering from the Tokyo Institute of Technology, Tokyo, Japan, in 2005, 2007, and 2016, respectively. In April 2007, he joined Nippon Telegraph and Telephone (NTT) Photonics Laboratories (now NTT Device Innovation Center), Japan. He is engaged in the research and development of optical semiconductor devices and integrated devices for optical communications systems. He is a Senior Member of the IEEE Photonics Society, and a Member of the Japan Society of Applied Physics and the Institute of Electronics, Information and Communication Engineers of Japan.

Takaaki Kakitsuka (Member, IEEE) was born in Kumamoto, Japan, in 1971. He received the B.S. and M.S. degrees in physics and the Dr. Eng. degree from Kyushu University, Fukuoka, Japan, in 1994, 1996, and 2012, respectively. In 1996, he joined NTT Opto-Electronics Laboratories, Nippon Telegraph and Telephone Corporation, Kanagawa, Japan. He was involved in research on semiconductor lasers and optical integrated devices at NTT Corporation from 1996 to 2019. In 2019, he became an Associate Professor at the Graduate School of Information, Production and Systems, Waseda University, Fukuoka, Japan. He has been involved in research on semiconductor lasers and their information communication system applications. He is a member of the IEICE, JSAP, and the Physical Society of Japan.

Shinji Matsuo (Fellow, IEEE) received the B.E. and M.E. degrees in electrical engineering from Hiroshima University, Hiroshima, Japan, in 1986 and 1988, respectively, and the Ph.D. degree in electronics and applied physics from the Tokyo Institute of Technology, Tokyo, Japan, in 2008. In 1988, he joined NTT Optoelectronics Laboratories, where he researched photonic functional devices using multiple quantum well pin modulators and VCSELs. In 1997, he researched optical networks using WDM technologies with NTT Network Innovation Laboratories. Since 2000, he has been researching high-speed tunable optical filters and lasers with NTT Photonics Laboratories, Atsugi, Japan, and NTT Device Technology Laboratories, Atsugi, Japan. He is a Senior Distinguished Researcher of NTT. He is a Member of the Japan Society for the Promotion of Science and IEICE, and Fellow of Optica.